Received 19 November 2025; Accepted 15 December 2025
https://doi.org/10.48612/letters/2026-1-37-42 https://elibrary.ru/velhgc

Influence of substitutional doping with boron, nitrogen and iron atoms on structural, electronic and optical properties of diamanes

A. A. Grekova, K. S. Grishakov, K. P. Katin, V. A. Kurakin†, M. M. Maslov

†fromkurakin@mail.ru

National Research Nuclear University "MEPhI", Moscow 115409, Russia

Abstract: The study presents a comprehensive theoretical investigation of the structural, electronic, and optical properties of lonsdaleite-type (AB stacking) diamane subjected to substitutional doping with boron, nitrogen, and iron atoms. All calculations were performed using the methods of density functional theory. We systematically examined the effects of impurity incorporation at concentrations of 7% and 13% on the diamane crystal lattice. The introduction of dopant atoms induces minimal lattice distortion, with changes in the lattice constant not exceeding 1% compared to pristine diamane. Specifically, boron and iron doping at 7% concentration results in approximately 1% lattice expansion, while nitrogen doping causes a 0.70% contraction. Simultaneous co-doping with nitrogen and boron atoms yields an average lattice parameter increase of 0.60%. The electronic band structure calculations demonstrate substantial modifications in the electronic properties of doped diamanes. While pristine AB-diamane exhibits a direct bandgap of ≈3 eV, nitrogen doping increases this value to 3.46 eV, whereas boron doping reduces it to 2.14 eV. Notably, simultaneous incorporation of boron and nitrogen atoms at 13% concentration, particularly when located in neighbouring diamane planes, induces a semiconductor-to-metal transition, suggesting potential applications in nanoelectronic devices. Iron doping at 7% concentration also significantly alters the electronic structure, creating partially filled energy bands that modify charge transport properties. Vibrational spectroscopy calculations provide characteristic signatures for experimental identification of dopants. The computed Raman and infrared spectra exhibit distinct peaks associated with impurity-carbon bond vibrations, enabling reliable detection of substitutional defects. Formation energy calculations indicate that nitrogen incorporation is most energetically favourable (0.44 eV), while iron doping is least favourable (7.37 eV). These findings provide valuable insights for the controlled synthesis and characterization of functionalized diamane materials with tailored electronic and optical properties for advanced technological applications.

Keywords: diamane, doping, electronic band structure, Raman spectra, IR spectra

Acknowledgments: *This study was supported by Ministry of Science and Higher Education of the Russian Federation (agreement/grant 075-15-2025-609).*

1. Introduction

Doping, i. e., the introduction of impurity atoms into the crystal lattice, is an effective way to control the electronic and optical characteristics of nanostructures and, in particular, 2D materials. For example, the introduction of substitutional atoms into the graphene crystal lattice leads to the opening of a band gap in its band structure. This approach allows stabilization of the graphene structure, creation of a p-n junction, and an increase in the charge carrier concentration [1–8]. In this case, doped graphene can be used in diodes, transistors, and other electronic devices [9]. The doping method with carbon or beryllium atoms is also used in 2D hydrogenated bilayer boron nitride with a wide band gap of about 6 eV. In this case, its dielectric gap decreases to 3 eV, and the absorption spectrum shifts from the ultraviolet range to the visible range [10]. Thus, such a 2D bilayer boron nitride can be applied as an active layer in optoelectronic devices.

Diamane is a unique quasi-two-dimensional structure that is obtained through the deposition of hydrogen or fluorine atoms on the outer sides of bigraphene [11–14]. Hydrogenation leads to the replacement of the interlayer van der Waals interaction in bilayer graphene with covalent bonds. Like its precursor, ideal diamane has several crystal lattice configurations, among which the energetically favourable ones are AA (diamond) and AB (lonsdaleite) stacking [11,12]. Its unique features also include a large band gap value (≈3 eV), mechanical strength [15,16], and flexibility [17]. Control of the electronic and optical characteristics of diamane through the introduction of various impurity atoms into its crystal lattice is also feasible. For example, nitrogen and boron doping of diamane with AA configuration leads to a change in the band gap width without a significant change in the lattice parameter [18]. This allows the use of AA-diamane for the formation of various types of lateral heterostructures [19], which can be used, for example, to study quantum effects of resonant tunnelling. It is also

known that a boron atom introduced into the crystal lattice of AB-diamane not only reduces its formation energy but also leads to a change in the band gap width [20]. Moreover, the close proximity of impurity atoms to the diamane surface, particularly F-diamane, unlike bulk diamond (the brightness of single-electron sources in bulk diamond is limited by its low quantum efficiency), allows for a significant increase in photon extraction efficiency, which is promising for applications in quantum technologies [21]. In the case of AB diamane, the influence of the type of impurity atoms and their position in the crystal lattice on electronic and optical characteristics has not been fully determined.

This theoretical study aims to determine the influence of impurity atoms of nitrogen, boron, and iron on the structural, electronic, and optical characteristics of diamane with AB stacking type using density functional theory calculations.

2. Materials and methods

When performing the calculations, Quantum Espresso software was used, which allows for the study of various properties of crystalline structures within the framework of density functional theory (DFT) [22, 23]. Structural optimization of the studied systems was performed using the Perdew-Wang (PW) exchange-correlation functional [24] with a plane wave basis set. It should be noted that in the structure of diamane, unlike graphite or bilayer graphene, interlayer interaction is realized predominantly through covalent bonds between carbon atoms of neighboring planes, while van der Waals interactions play a significantly smaller role. Therefore, we did not account for these corrections in our study. Calculation of electronic characteristics of optimized structures, such as band structure and density of electronic states, was also performed using the local density approximation (LDA) with the Perdew-Wang (PW) exchange-correlation functional [24] with a plane wave basis set. In the calculations of optical spectra, Troullier-Martins [25] norm-conserving pseudopotentials were used for all chemical elements employed. Cutoff energy values of 140 Ry and 640 Ry were chosen for wave functions and electron density, respectively. In reciprocal space, a $6\times6\times1$ k-point mesh constructed using the Monkhorst-Pack method [26] was used. The structural optimization process continued until the components of all forces acting on the atoms became less than 10^{-5} Ha/Bohr. In the direction perpendicular to the diamane plane, a "vacuum" of 30 Å was used to eliminate non-physical interactions between structure images due to the periodic boundary conditions. For calculations of the density of electronic states, the Blöchl tetrahedron method [27] was applied. For Brillouin zone integration, this method provides better determination of key features of the density of electronic states than the smearing method [28]. To determine phonon frequencies, Raman spectra, and IR spectra, the DFPT method [29] was applied.

To determine the substitution energy of a carbon atom (C) by an impurity atom (X) E_f^X, the following expression is used [30 – 33]:

$$E_f^X = E_{total}^X - E_{total}^C - \Sigma_X n_X \mu_X \quad (1)$$

where E_{total}^X is the total energy of diamane with an impurity atom incorporated into its crystal lattice, E_{total}^C is the total energy of the crystal lattice of ideal AB diamane, μ_X is the chemical potential of carbon or impurity atom X, n_X is the number of substituted atoms ($n_X<0$) and substituting ($n_X>0$) atoms of type X including carbon. The chemical potentials of the elements were evaluated by us at the same level of DFT theory as the energy per number of atoms in the simulation cell in its most stable phase: for carbon, diamond was chosen; for nitrogen, N_2 gas; for boron, α-rhombohedral phase of boron (B_{12}); for iron, bcc iron (α-Fe). The values of chemical potentials were (in eV per atom): $\mu_C=-155.718$, $\mu_N=-270.700$, $\mu_B=-91.418$, $\mu_H=-15.478$, $\mu_{Fe}=-540.175$. Note that under normal conditions, the most stable phase of carbon is graphite, not diamond. In our study, the choice of diamond as the reference phase is motivated by the fact that the structure of diamane is chemically and structurally closer to diamond (sp^3-hybridization of carbon atoms) than to graphite (sp^2-hybridization of carbon atoms). This choice allows for a more accurate assessment of the substitution energy within the studied system.

3. Results and discussions

In the present study, a 2×2 supercell of diamane with hexagonal symmetry was considered, containing 16 carbon atoms and 8 hydrogen atoms. We limited ourselves to considering configurations where single impurity atoms were three-fold coordinated. In the crystal lattice, there exists only one such non-equivalent position (see Fig. 1). In these configurations, along with the introduction of an impurity atom, a hydrogen atom is additionally removed. Since boron atoms can form only three covalent bonds, such a position in the crystal lattice of diamane is the most energetically favourable for them. Nitrogen atoms are also capable of forming three covalent bonds. DFT calculations showed that the most stable configurations are those in which nitrogen atoms incorporated into the AB-diamane structure have no bonds with hydrogen [20]. At the same time, iron atoms are capable of forming up to six covalent bonds. The use of identical configurations when introducing different impurity atoms allows for a more correct comparison of their substitution energies. In this case, the concentration of impurity atoms for the considered diamane structure is 7%.

Along with doping with a single impurity atom, we considered the case when nitrogen and boron atoms are simultaneously introduced into the AB-diamane lattice at different non-equivalent positions, shown in Fig. 2 (the

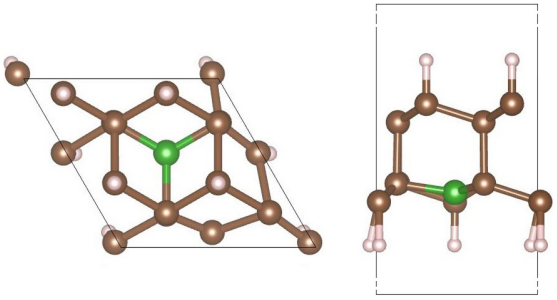

Fig. 1. (Color online) Crystal structures of AB-diamane with an incorporated impurity atom. Carbon atoms are shown in brown, hydrogen atoms in pink, and the impurity atom in green.

concentration of impurity atoms is 13%). We examined configurations where nitrogen and boron atoms are located both in the same diamane plane and in adjacent diamane planes. In the aforementioned structures, nitrogen-hydrogen bonds are present, which also affects the electronic characteristics of AB-diamane.

During the geometric optimization process, the following lattice constant values were obtained for the considered diamane supercell: ideal structure — 4.977 Å; diamane doped with boron atom — 5.033 Å; diamane doped with nitrogen atom — 4.942 Å; diamane doped with iron atom — 5.044 Å; diamane co-doped with nitrogen and boron atoms — 5.011 Å for the structure shown in Fig. 2 a; 5.006 Å for the structure shown in Fig. 2 b; 5.003 Å for the structure shown in Fig. 2 c. Analysis of the obtained data shows that the incorporation of single impurity atoms of boron or iron into the considered diamane unit cell leads to a relative increase in the AB-diamane lattice constant by approximately 1% (see Table 1). The incorporation of nitrogen atoms leads to a decrease in the AB-diamane lattice parameter by 0.70%, while the simultaneous incorporation of nitrogen and boron atoms leads to an increase in the AB-diamane lattice parameter by an average of 0.59%. Thus, the largest distortion of the lattice constant is observed in the case of incorporating iron and boron atoms at a concentration of 7%.

Using Eq. (1), the substitution energies of carbon atoms by impurity atoms in the AB-diamane crystal lattice were calculated (see Table 1). The incorporation of single nitrogen atoms is the most energetically favourable, while the incorporation of single iron atoms is the least favourable. Note that the high substitution energy suggests that iron doping may require special experimental conditions (elevated temperatures, ion implantation methods, or other non-equilibrium synthesis methods). In this regard, iron can be considered as a promising dopant only with specialized synthesis technologies, which limits its practical application compared to boron and nitrogen.

Table 1. Values for the formation energy and the lattice parameter mismatch $\Delta a = (l - l_0)/l_0 \cdot 100\%$ (l_0 is the lattice constant of the ideal structure) for various types of impurities in AB-diamane.

Impurity	B	N	Fe	B + N (Fig. 2 a)	B + N (Fig. 2 b)	B + N (Fig. 2 c)
Δa, %	1.13	−0.70	1.35	0.68	0.58	0.52
E_f^X, eV	1.93	0.44	7.37	3.79	2.86	2.27

Calculations of the electronic band structure for doped AB-diamanes were performed. AB-diamane is a direct bandgap wide-bandgap semiconductor with a bandgap of $E_g = 3.01$ eV (see Fig. 3 a). The obtained band gap of ideal AB-diamane agrees well with the values previously obtained using the PBE functional (3.04 eV [34], 3.01 eV [36]). For nitrogen-doped diamane, the E_g value increases to 3.46 eV (see Fig. 3 c), which is in good agreement with the value previously calculated using the PBE functional (3.43 eV [34]). In turn, the incorporated boron atom reduces E_g to 2.14 eV due to the formation of an energy band above the Fermi level with a width of ≈0.55 eV, which is separated from the higher-energy bands by approximately 0.10 eV (see Fig. 3 b). AB-diamane doped with a single nitrogen or boron atom remains a direct bandgap semiconductor. It should be noted that doping of AB-diamane with single nitrogen and boron atoms (concentration of 7%) leads to a similar change in the electronic structure as in the hexagonal lattice of AA-diamane (concentration of 6%). In particular, boron atom incorporation in both cases causes a decrease, while nitrogen atom incorporation causes an increase in the band gap [18]. The incorporation of an iron atom into the AB-diamane structure leads to the formation of an almost filled energy band at zero temperature with a width of ≈0.70 eV, which is separated from the higher-energy unfilled band with a width of ≈0.45 eV by a band energy gap of ≈0.72 eV (see Fig. 3 d).

Simultaneous incorporation of nitrogen and boron atoms in the case of configurations shown in Fig. 2 b, c (corresponding band structures are shown in Fig. 4 b, c) leads to the formation of a partially filled band with a width of ≈0.40 eV (for the configuration in Fig. 2 b) and ≈0.28 eV (for the configuration in Fig. 2 c), which is separated from the unfilled energy band by a band energy gap of 0.56 eV (for the configuration in Fig. 2 b) and 0.48 eV (for the configuration

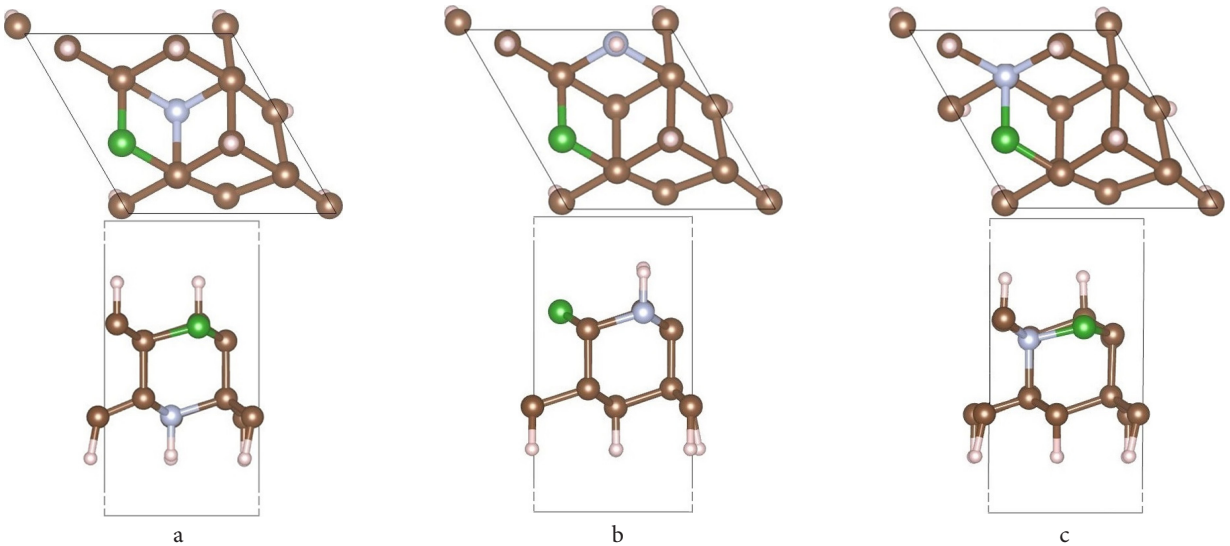

Fig. 2. (Color online) Crystal structures of AB-configuration diamane from top and side views with doped nitrogen and boron atoms. Carbon atoms are shown in brown, hydrogen atoms in pink, boron atom in green, and nitrogen atom in blue.

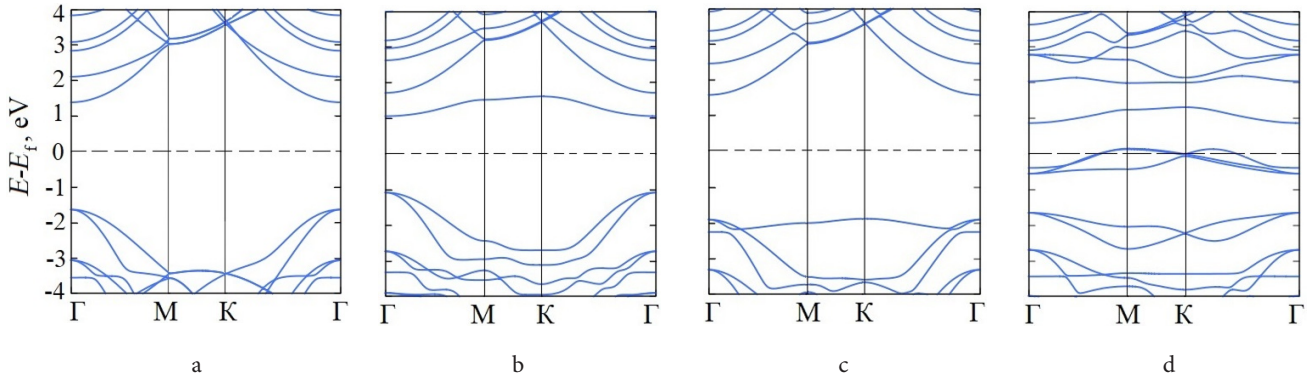

Fig. 3. Band structure: pristine crystal lattice of AB-diamane (a); boron-doped crystal lattice of AB-diamane (b); nitrogen-doped crystal lattice of AB-diamane (c); iron-doped crystal lattice of AB-diamane (d).

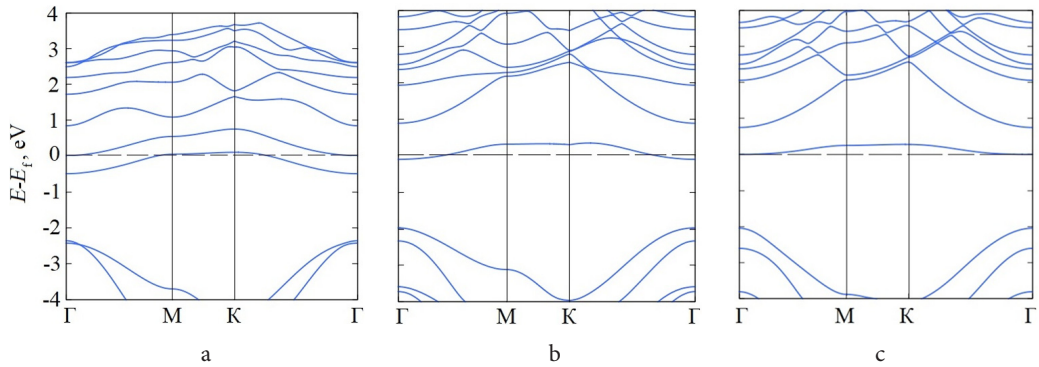

Fig. 4. Band structures of AB-diamanes with configurations of crystal lattices shown in: Fig. 2 a (a); Fig. 2 b (b); Fig. 2 c (c).

in Fig. 2 c). In the case of the structure shown in Fig. 2 a, analysis of its corresponding band structure (Fig. 4 a) allows us to conclude that the nature of conductivity changes from semiconducting to metallic. At the same time, for example, doping of fluorinated diamane with nitrogen and boron atoms leads to a decrease in the band gap from 4.04 down to 3.03 eV without transition to the metallic state [35].

Raman and IR spectroscopy are among the methods for identifying the presence of impurity atoms in the crystal lattice of various materials. In the present study, IR and Raman spectra were calculated for AB-diamanes in the presence of nitrogen and boron impurity atoms. The calculation results are shown in Figs. 5 – 7.

In the case of boron-doped AB-diamane, an additional peak of lower intensity appears in the Raman spectrum at 667 cm^{-1}. The peak at 1317 cm^{-1}, corresponding to vibrations of bonds between carbon atoms, splits into two peaks upon boron atom incorporation at frequencies of 1277 cm^{-1} (vibrations of bonds between carbon atoms) and 1406 cm^{-1} (vibrations of bonds between carbon and boron). In the IR spectrum of boron-doped AB-diamane, an additional peak appears at 1406 cm^{-1} with the highest intensity, corresponding to vibrations between boron and carbon. In the case of nitrogen-doped AB-diamane, the Raman spectrum shows that the peak at 1317 cm^{-1} splits into two peaks at 1258 cm^{-1} and 1354 cm^{-1}, which correspond to vibrations of bonds between carbon atoms. The peak at 1258 cm^{-1} corresponds to C-C bond vibrations in the direction perpendicular to the diamane planes. The peak at 1354 cm^{-1} corresponds to C-C bond vibrations in the direction along the diamane planes. In the IR spectrum of nitrogen-doped AB-diamane, the peak at 1139 cm^{-1} splits into two peaks at 1267 cm^{-1} (vibrations of bonds between carbon atoms) and 1036 cm^{-1}, with the latter having the highest intensity in the spectrum and corresponding to vibrations between nitrogen and carbon. The incorporation of nitrogen or boron atoms into the AB-diamane lattice has a negligible effect on the high-frequency hydrogen-carbon bond vibration.

4. Conclusion

The calculation results showed that in the case of the hexagonal unit cell of AB-diamane, doping with a single type of atom (nitrogen, boron, or iron) at a concentration of 7% and doping with nitrogen and boron atoms simultaneously (impurity concentration of 13%) leads to a negligible change in the lattice constant by ≤1%. The greatest change in the lattice constant is observed when doping the AB-diamane crystal lattice with nitrogen and iron atoms, while simultaneous incorporation of nitrogen and boron atoms leads to minimal distortion of the lattice parameter. The most energetically favourable is the incorporation of nitrogen atoms (0.44 eV) at a concentration of 7% into the AB-diamane crystal lattice, while iron doping (7.37 eV) is the least energetically favourable.

Doping allows for significant modification of the electronic properties of AB-diamane. In particular, simultaneous incorporation of nitrogen and boron atoms at a concentration of 13% in a configuration where they are located in neighbouring planes of the diamane crystal

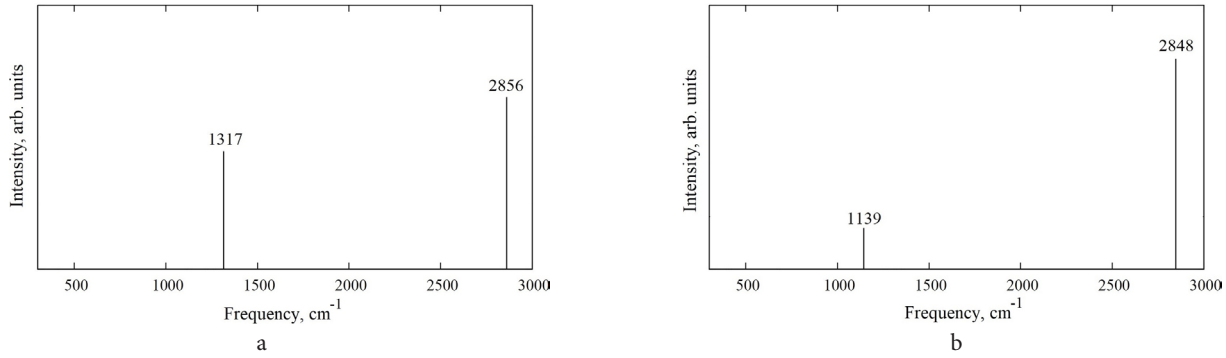

Fig. 5. Raman (a) and IR (b) spectra of pristine AB-diamane.

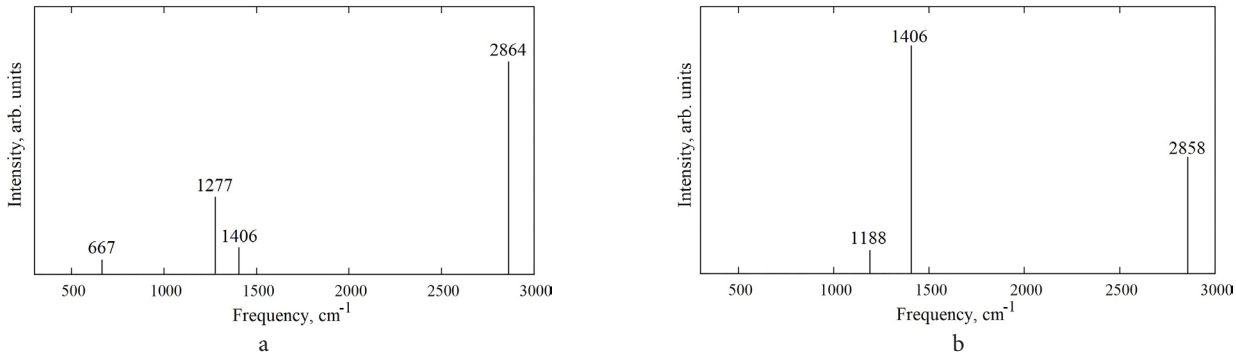

Fig. 6. Raman (a) and IR (b) spectra of AB-diamane doped with a boron atom.

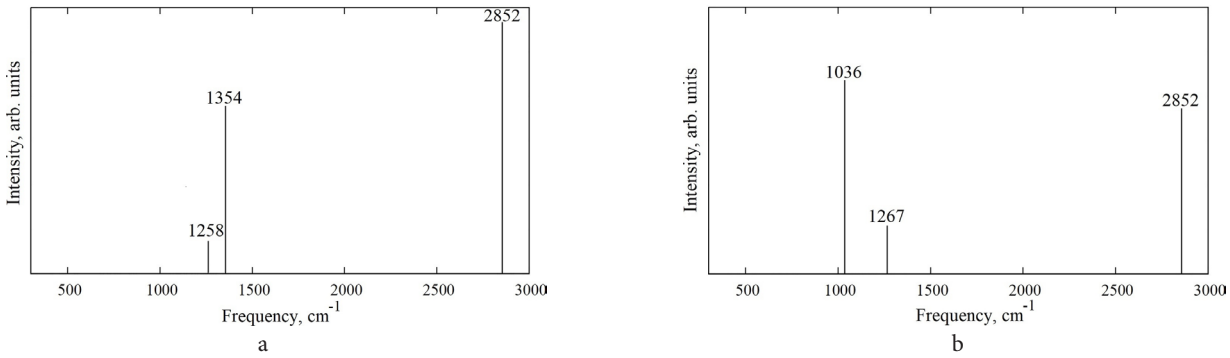

Fig. 7. Raman (a) and IR (b) spectra of AB-diamane doped with a nitrogen atom.

lattice without covalent interaction between them results in metallic properties. This can be useful in designing various nanoelectronic devices. The Raman and IR spectra obtained in this study showed that valence vibrations associated with changes in bonds between boron and carbon atoms, as well as carbon and nitrogen, correspond to characteristic peaks. In the IR spectra, the presence of substitutional atoms manifests itself in the appearance of pronounced peaks with the highest intensity, making it possible to experimentally determine the presence of such crystal lattice defects in AB-diamane.

References

1. L. A. Varlamova, S. V. Erohin, P. B. Sorokin, Formation of Ultrathin Diamond Films on Metal Substrates via Graphene-Metal Bonding, J. Phys. Chem. Lett. 15 (2024) 11927–11931.
2. M. D. Bhatt, H. Kim, G. Kim, Various defects in graphene: a review, RSC Adv. 12 (2022) 21520 – 21547.
3. M. T. T. Moghadam, K. Cysewska, Facile synthesis and characterization of graphene and N-doped graphene by CVD method from liquid precursors for promising electrode materials, MSEB. 302 (2024) 117254.
4. H. Wang, C. Zhao, L. Liu, Z. Xu, J. Wei, W. Wang, X. Bai, E. Wang, Towards the controlled CVD growth of graphitic B-C-N atomic layer films: The key role of B-C delivery molecular precursor, Nano Res. 9 (2016) 1221–1235.
5. K. M. Alanezi, I. Ahmad, S. AlFaify, I. Ali, A. Mohammad, M. S. Jabir, H. Majdi, F. M. Almutairi, A review of advanced heteroatom-doped graphene and its derivatives materials for photocatalytic applications, JIEC. 143 (2025) 1 – 32.
6. G. Deokar, J. Jin, U. Schwingenschlogl, P. M. F. J. Costa, Chemical vapor deposition-grown nitrogen-doped graphene's synthesis, characterization and applications, Npj 2D Mater. Appl. 6 (2022) 14.
7. M. K. Ubhi, M. Kaur, J. K. Grewal, V. K. Sharma, Phosphorous- and Boron-doped Graphene-based nanomaterials for Energy-Related Applications, Mater. 16 (2023) 1155.
8. P. Rani, V. K. Jindal, Designing band gap of graphene by B and N dopant atoms, RSC Advances. 3 (2013) 802 – 812.
9. K. A. Krylova, J. A. Baimova, R. T. Murzaev, R. R. Mulyukov,

Energy exchange between discrete breathers in graphene in thermal equilibrium, Phys. Lett. A. 383 (2019) 1583–1588.
10. J. Li, Y. Du, M. Zhang, J. Zhang, J. Mu, L. Gao, C. Zhang, X. Dai, Y. Ma, Tuning the electronic and optical properties of two-dimensional hydrogenated c-BN nanosheets by Be and C dopants and vacancy defects, Chem. Phys. 555 (2022) 111441.
11. B. Liu, E. Emmanuel, T. Liang, B. Wang, Advancements in theoretical and experimental investigations on diamanes materials, Nanoscale. 15 (2023) 10498–10512.
12. P. B. Sorokin, B. I. Yakobson, Two-Dimensional Diamond-Diamane: Curent State and Further Prospects, Nano Lett. 21 (2021) 5475 – 5484.
13. G. Qin, L. Wu, H. Gou, Diamane: design, synthesis, properties, and challenges, Functional Diamond. 1 (2021) 83 – 92.
14. F. Piazza, M. Monthioux, P. Puech, I. C. Gerber, K. Gough, Progress on Diamane and Diamanoid Thin Fim Pressureless Synthesis, MDPI 7 (2021) 9.
15. P. V. Polyakova, L. Kh. Galiakhmetova, R. T. Murzaev, D. S. Lisovenko, J. A. Baimova, Elastic properties of diamane, Lett. Mater. 13 (2023) 171–176.
16. P. V. Polyakova, R. T. Murzaev, J. A. Baimova, Mechanical properties of diamane: Orientation dependence of strength and fracture strain, Appl. Surf. Sci. 681 (2025) 161441.
17. B. Mortazavi, F. Shojaei, B. Javvaji, M. Azizi, H. Zhan, T. Ranczuk, X. Zhuang, First-principles investigation of mechanical, electronic and optical properties of H-, F- and Cl-diamane, Appl. Surf. Sci. 528 (2020) 147035.
18. A. A. Grekova, K. S. Grishakov, K. P. Katin, M. M. Maslov, Influence of Substitutional Doping by Boron and Nitrogen Atoms on Electronic and Optical Characteristics of Diamanes, J. Struct. Chem. 66 (2025) 230 – 239.
19. K. S. Grishakov, V. B. Merinov, K. P. Katin, M. M. Maslov, Electronic characteristics of diamanes and diamane-based heterojunctions, Phys. E: Low-dimensional Systems and Nanostructures. 171 (2025) 116248.
20. C. Niu, Y. Cheng, K. Yang, J. Zhang, H. Zhang, Z. Zeng, X. Wang, Boron-dopant enhanced stability of diamane with tunable band gap, J. Phys.: Condens. Matter. 32 (2020) 135503.
21. L. Yan, S. Cheng, Y. Ku, D. Wang, T. Liu, X. Li, Z. Zhang, C. Shan, Intralevel Optical Transitions of X*V* (X*V* = B*V*, Si*V*, and N*V*) Centers in Fluorinated Diamane, Nano Lett. 25 (2025) 4818 – 4824.
22. P. Giannozzi, O. Andreussi, T. Brumme, O. Bunau, M. Buongiorno Nardelli, M. Calandra, R. Car, C. Cavazzoni, D. Ceresoli, M. Cococcioni, N. Colonna, I. Carnimeo, A. Dal Corso, S. de Gironcoli, P. Delugas, R. A. DiStasio, A. Ferretti, A. Floris, G. Fratesi, G. Fugallo, R. Gebauer, U. Gerstmann, F. Giustino, T. Gorni, J. Jia, M. Kawamura, H.-Y. Ko, A. Kokalj, E. Küçükbenli, M. Lazzeri, M. Marsili, N. Marzari, F. Mauri, N. L. Nguyen, H.-V. Nguyen, A. Otero-de-la-Roza, L. Paulatto, S. Poncé, D. Rocca, R. Sabatini, B. Santra, M. Schlipf, A. P. Seitsonen, A. Smogunov, I. Timrov, T. Thonhauser, P. Umari, N. Vast, X. Wu, S. Baroni, Advanced capabilities for materials modelling with Quantum ESPRESSO, J. Phys.: Condens. Matter, 29 (2017) 465901.
23. P. Giannozzi, S. Baroni, N. Bonini, M. Calandra, R. Car, C. Cavazzoni, D. Ceresoli, G. L. Chiarotti, M. Cococ cioni, I. Dabo, A. Dal Corso, S. de Gironcoli, S. Fabris, G. Fratesi, R. Gebauer, U. Gerstmann, C. Gougous sis, A. Kokalj, M. Lazzeri, L. Martin-Samos, N. Marzari, F. Mauri, R. Mazzarello, S. Paolini, A. Pasqua rello, L. Paulatto, C. Sbraccia, S. Scandolo, G. Sclauzero, A. P. Seitsonen, A. Smogunov, P. Umari, R. M. Wentz covitch, QUANTUM ESPRESSO: a modular and open-source software project for quantum simulations of materials, J. Phys.: Condens. Matter. 21 (2009) 395502.
24. J. P. Perdew, Y. Wang, Accurate and simple analytic representation of the electron-gas correlation energy, Phys. Rev. B. 45 (1992) 13244–13249.
25. N. Troullier, J. L. Martins, Efficient pseudopotentials for plane-wave calculations, Phys. Rev. B. 43 (1991) 1993 – 2006.
26. H. J. Monkhorst, J. D. Pack, Special points for Brillouin-zone integrations, Phys. Rev. B. 13 (1976) 5188 – 5192.
27. P. E. Blöchl, O. Jepsen, O. K. Andersen, Improved tetrahedron method for Brillouin-zone integrations, Phys. Rev. B. 49 (1994) 16223–16233.
28. M. Y. Toriyama, A. M. Ganose, M. Dylla, S. Anand, J. Park, M. K. Brod, J. M. Munro, K. A. Persson, A. Jain, G. J. Snyder, How to analyze a density of states, Mater. Today Electron. 1 (2022) 100002.
29. S. Baroni, S. de Gironcoli, A. Dal Corso, P. Giannozzi, Phonons and related crystal properties from density functional perturbation theory, Rev. Mod. Phys. 73 (2001) 515 – 562.
30. A. Kesorn, R. Hunkao, C.N. Talang, C. Cholsuk, A. Sinsarp, T. Vogl, S. Suwanna, S. Yuma, Formation energy prediction of neutral single-atom impurities in 2D materials using tree-based machine learning, Mach. Learn.: Sci. Technol. 5 (2024) 035039.
31. B. Huang, H. Lee, Defect and impurity properties of hexagonal boron nitride: A first-principles calculation, Phys. Rev. B. 86 (2012) 245406.
32. B. Huang, H. J. Xiang, S. H. Wei, Controlling doping in graphene through a SiC substrate: A first-principles study, Phys. Rev. B. 83 (2011) 161405.
33. S. Y. Davydov, Energy of substitution of atoms in the epitaxial graphene-buffer layer-SiC substrate system, Phys. of the Sol. St. 54 (2012) 875 – 882.
34. C. Niu, J. Zhang, H. Zhang, J. Zhao, W. Xia, Z. Zeng, X. Wang, Configuration stability and electronic properties of diamane with boron and nitrogen dopants, Phys. Rev. B. 105 (2022) 174106.
35. Q. Yu, N. Gao, H. Li, First-principles study on electronic and mechanical properties of boron and nitrogen co-doped fluorinated diamane, Diamond Relat. Mater. 146 (2024) 111253.
36. L. Ge, H. Liu, J. Wang, H. Huang, Z. Cui, Q. Huang, Z. Fu, Y. Lu, Properties of diamane anchored with different groups, Phys. Chem. Chem. Phys. 23 (2021) 14195.